



MacTaggart, D. , Vergori, L. and Quinn, J. (2017) Braginskii magnetohydrodynamics for arbitrary magnetic topologies: coronal applications. *Journal of Fluid Mechanics*, 826, pp. 615-635. (doi:[10.1017/jfm.2017.463](https://doi.org/10.1017/jfm.2017.463))

This is the author's final accepted version.

There may be differences between this version and the published version. You are advised to consult the publisher's version if you wish to cite from it.

<http://eprints.gla.ac.uk/143214/>

Deposited on: 29 June 2017

Enlighten – Research publications by members of the University of Glasgow  
<http://eprints.gla.ac.uk>

# Braginskii MHD for arbitrary magnetic topologies: coronal applications

D. MacTaggart<sup>1</sup>†, L. Vergori<sup>1,2</sup> and J. Quinn<sup>1</sup>

<sup>1</sup>School of Mathematics and Statistics, University of Glasgow, Glasgow, G12 8SQ, UK

<sup>2</sup>Dipartimento di Ingegneria, Università di Perugia, via Goffredo Duranti 93, 06125, Perugia, Italy

(Received xx; revised xx; accepted xx)

We investigate single-fluid magnetohydrodynamics (MHD) with anisotropic viscosity, often referred to as Braginskii MHD, with a particular eye to solar coronal applications. First, we examine the full Braginskii viscous tensor in the single-fluid limit. We pay particular attention to how the Braginskii tensor behaves as the magnetic field strength vanishes. The solar corona contains a magnetic field with a complex and evolving topology, so the viscosity must revert to its isotropic form when the field strength is zero, e.g. at null points. We highlight that the standard form in which the Braginskii tensor is written is not suitable for inclusion in simulations as singularities in the individual terms can develop. Instead, an altered form, where the parallel and perpendicular tensors are combined, provides the required asymptotic behaviour in the weak-field limit. We implement this combined form of the tensor into the Lare3D code, which is widely used for coronal simulations. Since our main focus is the viscous heating of the solar corona, we drop the drift terms of the Braginskii tensor. In a stressed null point simulation, we discover that small-scale structures, which develop very close to the null, lead to anisotropic viscous heating at the null itself (that is, heating due to the anisotropic terms in the viscosity tensor). The null point simulation we present has a much higher resolution than many other simulations containing null points so this excess heating is a practical concern in coronal simulations. To remedy this unwanted heating at the null point, we develop a model for the viscosity tensor that captures the most important physics of viscosity in the corona: parallel viscosity for strong field and isotropic viscosity at null points. We derive a continuum model of viscosity where momentum transport, described by this viscosity model, has the magnetic field as its preferred orientation. When the field strength is zero, there is no preferred direction for momentum transport and viscosity reverts to the standard isotropic form. The most general viscous stress tensor of a (single-fluid) plasma satisfying these conditions is found. It is shown that the Braginskii model, without the drift terms, is a specialization of the general model. Performing the stressed null point simulation with this simplified model of viscosity reveals very similar heating profiles compared to the full Braginskii model. The new model, however, does not produce anisotropic heating at the null point, as required. Since the vast majority of coronal simulations use only isotropic viscosity, we perform the stressed null point simulation with isotropic viscosity and compare the heating profiles to those of the anisotropic models. It is shown that the fully isotropic viscosity can over-estimate the viscous heating by an order of magnitude.

**Key words:** MHD and Electrohydrodynamics

---

† Email address for correspondence: david.mactaggart@glasgow.ac.uk

## 1. Introduction

The large-scale dynamics of the solar corona are normally modelled by a single-fluid continuum description of a plasma. *Magnetohydrodynamics* (MHD) represents a union of fluid mechanics and electromagnetism and has been successfully applied to describe a vast range of solar phenomena (e.g. Priest 2014). One aspect, however, that has received little attention in coronal applications is the form of the viscosity tensor. The vast majority of applications use the standard viscous stress tensor of an isotropic Newtonian fluid. In a magnetized plasma, however, this viscosity is not correct as it ignores the influence of the magnetic field. Instead, *anisotropic viscosity* is required for plasmas like the solar corona. Other astrophysical applications have highlighted the importance of anisotropic viscosity. Studies of intrachuster (e.g. Schekochihin & Cowley 2006; Kunz et al. 2012; Santos-Lima et al. 2014, 2016; Berlock & Pessah 2015) and solar wind (e.g. Bale et al. 2009) plasmas have demonstrated that instabilities due to anisotropic effects can have a large influence on dynamics.

One important aspect of the coronal magnetic field is that it has a complex and evolving topology. Magnetic topology depends on magnetic *null points*, i.e. points where the magnetic field strength is zero. Null points appear and disappear as the field evolves and are important locations for magnetic reconnection and dynamic phenomena in the solar corona. Since the magnetic field reduces to zero at these locations, anisotropic viscosity must ‘switch’ to the fully isotropic case at null points.

The seminal work of Braginskii (1965) introduced a model for how the viscous stress tensor of a magnetized plasma can be expressed. When MHD is combined with an anisotropic viscosity (normally Braginskii viscosity in the strong-field limit) it is referred to as *Braginskii MHD*. In this paper, we examine the form of Braginskii MHD suitable for coronal (and other solar) applications. We shall pay particular attention to how the Braginskii model behaves as a null point is approached and how the viscous stress is best expressed for implementation in simulations. We implement the Braginskii tensor in a simulation and show that unwanted heating at the null point, due to the anisotropic parts of the tensor, develops. As a remedy to this, we develop a viscous stress tensor that captures the main physics of viscosity in the corona and does not exhibit the numerical problem mentioned above. We derive the most general stress tensor that satisfies the required physics. It is shown that the Braginskii tensor, without the drift terms, is a special case of this general tensor. We simplify the general tensor to one that captures the switch from parallel viscosity in strong magnetic fields to isotropic viscosity at null points. This simple switching model does not produce the unwanted anisotropic heating at the null point, as required.

After the theory of the viscous stress tensors is presented, we present the results of the simulations of stressed null points. These results are presented in the same section for ease of comparison. A study of the viscous heating reveals that assuming the viscosity is isotropic (as in most current coronal models) can produce heating that is orders of magnitude different from anisotropic models. The paper concludes with a discussion of the results and future applications.

## 2. Braginskii viscous stress

As mentioned above, Braginskii (1965) describes the form of anisotropic viscosity in a magnetized plasma. Starting from kinetic theory and building to a two-fluid description of the plasma, viscosity expressions are given for the electron and ion fluids. For each species, there are five viscosity coefficients corresponding to the five components of the viscous

stress tensor with respect to an orthogonal basis, say  $\mathscr{W}$ , of the five-dimensional Euclidean space of symmetric traceless tensors (endowed with the scalar product  $\mathbf{A} : \mathbf{B} = \text{tr}(\mathbf{A}^T \mathbf{B})$ ) (e.g. Kotelnikov 2012). For the ion fluid, which is used in the single-fluid description of the plasma, the Braginskii viscous stress can be written as

$$\boldsymbol{\sigma}_{\text{brag}} = \eta_0 \mathbf{W}^{(0)} + \eta_1 \mathbf{W}^{(1)} + \eta_2 \mathbf{W}^{(2)} - \eta_3 \mathbf{W}^{(3)} - \eta_4 \mathbf{W}^{(4)}, \quad (2.1)$$

where  $\eta_0$  to  $\eta_4$  are the viscosity coefficients that we shall discuss shortly. Following the layout in Hogan (1984), the five basis vectors in  $\mathscr{W}$  read

$$\mathbf{W}^{(0)} = \frac{3}{2}(\mathbf{W}\mathbf{b} \cdot \mathbf{b}) \left( \mathbf{b} \otimes \mathbf{b} - \frac{1}{3}\mathbf{I} \right), \quad (2.2)$$

$$\mathbf{W}^{(1)} = (\mathbf{I} - \mathbf{b} \otimes \mathbf{b})\mathbf{W}(\mathbf{I} - \mathbf{b} \otimes \mathbf{b}) + \frac{1}{2}(\mathbf{W}\mathbf{b} \cdot \mathbf{b})(\mathbf{I} - \mathbf{b} \otimes \mathbf{b}), \quad (2.3)$$

$$\mathbf{W}^{(2)} = (\mathbf{I} - \mathbf{b} \otimes \mathbf{b})\mathbf{W}(\mathbf{b} \otimes \mathbf{b}) + (\mathbf{b} \otimes \mathbf{b})\mathbf{W}(\mathbf{I} - \mathbf{b} \otimes \mathbf{b}), \quad (2.4)$$

$$\mathbf{W}^{(3)} = \frac{1}{2}\mathbf{Z}\mathbf{W}(\mathbf{I} - \mathbf{b} \otimes \mathbf{b}) - \frac{1}{2}(\mathbf{I} - \mathbf{b} \otimes \mathbf{b})\mathbf{W}\mathbf{Z}, \quad (2.5)$$

$$\mathbf{W}^{(4)} = (\mathbf{Z}\mathbf{W}\mathbf{b}) \otimes \mathbf{b} + \mathbf{b} \otimes (\mathbf{Z}\mathbf{W}\mathbf{b}). \quad (2.6)$$

In equations (2.2) to (2.6),  $\mathbf{b} = \mathbf{B}/|\mathbf{B}|$  is the unit vector in the direction of the magnetic field and  $\mathbf{I}$  is the identity tensor.  $\mathbf{W}$  is the traceless tensor given by

$$\mathbf{W} = \nabla \mathbf{u} + (\nabla \mathbf{u})^T - \frac{2}{3}(\nabla \cdot \mathbf{u})\mathbf{I} = 2 \left[ \mathbf{D} - \frac{1}{3}\text{tr}(\mathbf{D})\mathbf{I} \right], \quad (2.7)$$

where  $\mathbf{D}$  is the strain rate tensor.  $\mathbf{Z}$  is the tensor with components  $Z_{ij} = \epsilon_{ikj}b_k$ , where  $\epsilon_{ikj}$  are the components of the Ricci alternator.

Braginskii (1965) gives expressions for the (ion) transport coefficients in terms of the dimensionless parameter  $x_i = \omega_i \tau_i$ , where  $\omega_i (= |e\mathbf{B}|/m_i)$ , with  $e$  being the elementary charge and  $m_i$  the ion mass) is the ion cyclotron frequency and  $\tau_i$  is the ion-ion collision time in an unmagnetized plasma. For a fully ionized hydrogen plasma, we could use the subscript  $p$  to refer to *proton* explicitly. In this paper, however, we shall stick to the notation of Braginskii (1965). The viscosity coefficients are approximate expressions found from a kinetic description of the plasma (see Spitzer & Härm 1953; Epperlein & Haines 1986). If we fix  $\eta_0$ , the approximate viscosity expressions are

$$\eta_2 = \frac{\eta_0}{\Delta} \left( \frac{6}{5}x_i^2 + 2.23 \right), \quad \eta_1 = \eta_2(2x_i), \quad (2.8)$$

$$\eta_4 = \frac{\eta_0}{\Delta} x_i(x_i^2 + 2.38), \quad \eta_3 = \eta_4(2x_i), \quad (2.9)$$

where

$$\Delta = 2.23 + 4.03x_i^2 + x_i^4. \quad (2.10)$$

Each of the above tensors has a physical interpretation.  $\eta_0 \mathbf{W}^{(0)}$  represents the viscosity parallel to the magnetic field.  $\eta_1 \mathbf{W}^{(1)} + \eta_2 \mathbf{W}^{(2)}$  represents the perpendicular contribution and  $-\eta_3 \mathbf{W}^{(3)} - \eta_4 \mathbf{W}^{(4)}$ , the drift contribution (Hogan 1984).

Before considering the behaviour of the Braginskii viscous stress in particular field strength limits, notice that

$$\mathbf{W} = \mathbf{W}^{(0)} + \mathbf{W}^{(1)} + \mathbf{W}^{(2)}. \quad (2.11)$$

Since  $\mathbf{W}^{(3)}$  and  $\mathbf{W}^{(4)}$  do not appear in equation (2.11), they are both orthogonal to  $\mathbf{W}$ . Hence, they are not true viscous stresses as they produce no viscous dissipation. Further, since  $\mathbf{W}^{(3)}$  and  $\mathbf{W}^{(4)}$  contain odd multiples of  $\mathbf{b}$ , making the switch  $\mathbf{b} \rightarrow -\mathbf{b}$  changes

the sign of these tensors. In standard single-fluid MHD, the equations are invariant to the transformation  $\mathbf{b} \rightarrow -\mathbf{b}$ . Including the drift terms breaks this symmetry. Since our primary focus is the large-scale solar corona, where the effects of magnetic field polarization are not particularly important (e.g. Hollweg 1985; Bogaert & Goossens 1991), we shall ignore the drift terms in the main body of this paper. Later we shall demonstrate that the remaining terms in the Braginskii viscous tensor have a clear interpretation at the (single-fluid) continuum level in terms of the distribution of momentum transport.

Strictly speaking, the perpendicular terms should also be dropped, along with the drift terms, for coronal applications. However, as we shall demonstrate in some analysis later, it will be necessary to write the perpendicular and parallel terms in a combined and so we must retain the perpendicular terms.

### 2.1. Limit of strong magnetic field

All of the applications of Braginskii MHD cited in the Introduction are in the strong-field regime ( $x_i \gg 1$ ). By considering equations (2.8) to (2.9), it is clear that in the strong-field limit, the parallel viscosity dominates and the viscous stress tensor can be simplified to

$$\boldsymbol{\sigma} = \eta_0 \mathbf{W}^{(0)} = \frac{3}{2} \eta_0 (\mathbf{W} \mathbf{b} \cdot \mathbf{b}) \left( \mathbf{b} \otimes \mathbf{b} - \frac{1}{3} \mathbf{I} \right). \quad (2.12)$$

In the solar corona, it is also the case that  $x_i \gg 1$ . For example, consider a relatively weak coronal field of 10G. Then it can be shown that  $x_i \sim 10^5$  (Hollweg 1986). Hence, equation (2.12) would apply throughout most of the corona.

Hollweg (1985) gives a physical interpretation of equation (2.12) as being due to small pressure anisotropies that develop as the flows evolve. He shows that equation (2.12) can be derived from assuming a diagonal pressure tensor and equations analogous to the double adiabatic equations (Chew, Goldberger & Low 1956). Hollweg (1986) extends the analysis of equation (2.12) to include the effects of resistivity. In doing this, he notes that the use of equation (2.12) would not be suitable for reconnection-type flows, like those described in Sonnerup & Priest (1975). Such flows involve the compression of the magnetic field to null points.

Compared to coronal models that use only isotropic viscosity, those with Braginskii viscosity are in the minority. Many of the earlier studies of Braginskii MHD in the corona are in the strong-field limit (e.g. van der Linden et al. 1988; Hood et al. 1989; Ofman et al. 1994; Ruderman et al. 1996). Several recent works study two dimensional null point reconnection in the incompressible regime (Craig 2010; Craig & Litvinenko 2010; Armstrong, Craig & Litvinenko 2011; Armstrong & Craig 2013, 2014). To deal with the concerns mentioned above, they interpolate between equation (2.12) when the field is strong and the standard expression for isotropic viscosity at null points. We shall now consider Braginskii viscosity in the limit  $|\mathbf{B}| \rightarrow 0$ .

### 2.2. Limit of weak magnetic field

The Braginskii tensors, as written in equations (2.2) to (2.4), are not in a suitable form for studying how the viscosity behaves in the limit  $|\mathbf{B}| \rightarrow 0$ . For example, let us momentarily consider only the parallel viscosity given by equation (2.12). Since the unit vector  $\mathbf{b}$  is not defined when  $|\mathbf{B}| = 0$ , we would require that  $\eta_0/|\mathbf{B}|^4 \rightarrow l \in \mathbb{R}$  as  $|\mathbf{B}| \rightarrow 0$ . However, since the parallel viscosity coefficient  $\eta_0$  is constant,  $\eta_0/|\mathbf{B}|^4$  is singular at null points. This means that, as we shall demonstrate shortly, we require combinations of  $\{\mathbf{W}^{(0)}, \mathbf{W}^{(1)}, \mathbf{W}^{(2)}\}$  in order to correctly describe Braginskii's model in

the limit  $|\mathbf{B}| \rightarrow 0$ . Before doing this, and in order to make the analysis clearer, we relabel the numerical values in the viscosity coefficients (2.8) and write

$$\eta_2 = \frac{\eta_0(a_1x_i^2 + a_2)}{x_i^4 + a_3x_i^2 + a_2}, \quad \eta_1 = \eta_2(2x_i). \quad (2.13)$$

We also write  $x_i = \alpha|\mathbf{B}|$ , with  $\alpha = |e|\tau_i/m_i$ . Therefore, the viscosity coefficients (2.13) can be written as

$$\eta_2(|\mathbf{B}|) = \frac{\eta_0(a_1\alpha^2|\mathbf{B}|^2 + a_2)}{\alpha^4|\mathbf{B}|^4 + a_3\alpha^2|\mathbf{B}|^2 + a_2}, \quad \eta_1(|\mathbf{B}|) = \eta_2(2|\mathbf{B}|). \quad (2.14)$$

From expressions (2.14), we deduce that as  $|\mathbf{B}| \rightarrow 0$ ,

$$\eta_1 \sim \eta_0 \left[ 1 + \frac{4(a_1 - a_3)}{a_2} \alpha^2 |\mathbf{B}|^2 - \frac{16(a_1 a_3 - a_3^2 + a_2)}{a_2^2} \alpha^4 |\mathbf{B}|^4 \right] + O(|\mathbf{B}|^6), \quad (2.15)$$

$$\eta_2 \sim \eta_0 \left[ 1 + \frac{a_1 - a_3}{a_2} \alpha^2 |\mathbf{B}|^2 - \frac{a_1 a_3 - a_3^2 + a_2}{a_2^2} \alpha^4 |\mathbf{B}|^4 \right] + O(|\mathbf{B}|^6). \quad (2.16)$$

Simplifying and rearranging equations (2.1) to (2.4) gives

$$\begin{aligned} \sigma_{\text{brag}} &= \frac{3\eta_0 + \eta_1 - 4\eta_2}{2|\mathbf{B}|^4} (\mathbf{W}\mathbf{B} \cdot \mathbf{B})(\mathbf{B} \otimes \mathbf{B}) \\ &\quad + \frac{\eta_1 - \eta_0}{2|\mathbf{B}|^2} (\mathbf{W}\mathbf{B} \cdot \mathbf{B})\mathbf{I} \\ &\quad + \frac{\eta_2 - \eta_1}{|\mathbf{B}|^2} [\mathbf{W}(\mathbf{B} \otimes \mathbf{B}) + (\mathbf{B} \otimes \mathbf{B})\mathbf{W}] \\ &\quad + \eta_1 \mathbf{W}. \end{aligned} \quad (2.17)$$

For equation (2.17) to be well defined at null points, we require

$$3\eta_0 + \eta_1 - 4\eta_2 \sim O(|\mathbf{B}|^4), \quad (2.18)$$

$$\eta_1 - \eta_0 \sim \eta_2 - \eta_1 \sim O(|\mathbf{B}|^2), \quad (2.19)$$

as  $|\mathbf{B}| \rightarrow 0$ . By virtue of expressions (2.15) and (2.16), it is clear that the asymptotic requirements (2.18) to (2.19) are satisfied. Hence, the Braginskii tensor (2.17) is well defined as  $|\mathbf{B}| \rightarrow 0$ .

For the implementation of Braginskii viscosity in simulations, the form given in equation (2.17) is recommended in order to make sure that there is no singular behaviour in the limit  $|\mathbf{B}| \rightarrow 0$ . As highlighted above, considering the Braginskii tensor written in the form of equation (2.1) could lead to singular behaviour in numerical implementations. A similar analysis for the drift terms is given in the Appendix.

### 3. Continuum description

The previous section highlights that in order for the Braginskii tensor to be implemented numerically in an application with a non-trivial magnetic topology, the individual tensors  $\mathbf{W}^{(i)}$  have to be combined. Hence, the physical interpretation of the individual  $\mathbf{W}^{(i)}$  can no longer be easily separated. For example, close to a null point there would be a mixture of effects due to the parallel, perpendicular and isotropic parts of the viscosity tensor (2.17). As we shall discover later, this will lead to numerical difficulties in null

point simulations. In the solar corona, the two main contributions of viscosity are parallel viscosity (in the strongly-magnetized plasma) and isotropic viscosity (at null points). It is therefore useful to have a model that can switch between these two limits in a consistent way. Such a model would be simpler to interpret in a complicated 3D coronal simulation and could prevent unwanted anisotropic heating at under-resolved null points. Again, we shall return to this issue later when considering an illustrative numerical example.

In this section we derive, at the continuum level, a general viscous tensor that is based on the required physics, namely, that momentum transport is bound to follow the direction of the magnetic field when the plasma is strongly magnetized and has no preferred direction when the field goes to zero at null points. We show that the Braginskii tensor (2.17) is a special case of this new tensor and also derive a simpler model that captures the parallel-isotropic switch which describes the main viscous contributions in the corona. We detail carefully how the orientation of momentum transport changes from a preferred direction (that of the magnetic field) to no preferred direction (the isotropic case).

### 3.1. General form

We start by considering the Cauchy stress tensor as the sum of three contributions

$$\boldsymbol{\sigma} = \boldsymbol{\sigma}_H + \boldsymbol{\sigma}_M + \boldsymbol{\sigma}_V. \quad (3.1)$$

The isotropic tensor

$$\boldsymbol{\sigma}_H = -p_s \mathbf{I}, \quad (3.2)$$

with  $p_s$  being the hydrostatic pressure, is the hydrostatic stress tensor. The second contribution is due to the Lorentz force which can be viewed as the elastic response of the magnetic field on the plasma. This force can be expressed as the divergence of the Maxwell stress tensor

$$\boldsymbol{\sigma}_M = \mu_0^{-1} \left[ \mathbf{B} \otimes \mathbf{B} - \frac{1}{2} (\mathbf{B} \cdot \mathbf{B}) \mathbf{I} \right]. \quad (3.3)$$

The combination of  $\boldsymbol{\sigma}_H$  and  $\boldsymbol{\sigma}_M$  represents the stress tensor for an inviscid plasma. To model the viscous stress tensor  $\boldsymbol{\sigma}_V$ , we assume that it depends on both the rate of strain and the distribution of the orientations of momentum transport relative to the magnetic field lines. We then assume that  $\boldsymbol{\sigma}_V$  is given by a constitutive relation of the form

$$\boldsymbol{\sigma}_V = \hat{\boldsymbol{\sigma}}_V(\mathbf{D}, \mathbf{H}, |\mathbf{B}|), \quad (3.4)$$

where, as before,  $\mathbf{D}$  is the strain rate tensor, and  $\mathbf{H}$  is a structure tensor describing the distribution of the orientations of momentum transport throughout the plasma. If  $\mathbf{H} = \mathbf{O}$ , as would be required if  $\mathbf{B} = \mathbf{0}$ ,  $\hat{\boldsymbol{\sigma}}_V(\mathbf{D}, \mathbf{O}, 0)$  gives the (isotropic) viscous stress tensor for non-magnetic plasmas.

### 3.2. Structure tensor

To derive a suitable form for the structure tensor  $\mathbf{H}$ , we shall borrow ideas that are more common in nonlinear elasticity and the theory of liquid crystals. We start by assuming that the magnetic field  $\mathbf{B}$  is non-zero throughout the plasma. Hence, the unit vector field  $\mathbf{b} = \mathbf{B}/|\mathbf{B}|$  gives the direction of the magnetic field at any point. Since, at kinetic lengthscales, particles are constrained to follow magnetic field lines when the field is strong, the direction of the magnetic field represents the preferred orientation of momentum transport in the plasma.

Next, we introduce an *orientation density function*  $f_{\mathbf{x}} : \mathbb{S}^2 \rightarrow \mathbb{R}^+$ ,  $\mathbb{S}^2$  being the

unit sphere, such that  $f_{\mathbf{x}}(\mathbf{t}) d\omega$  gives the probability that, at  $\mathbf{x} \in \mathbb{R}^3$ , the direction of momentum transport through  $\mathbf{x}$  orients along  $\mathbf{t}$  within the solid angle  $d\omega$ . The orientation density function  $f_{\mathbf{x}}$  must then satisfy the normalization condition

$$\frac{1}{4\pi} \int_{\mathbb{S}^2} f_{\mathbf{x}}(\mathbf{t}) d\omega = 1. \quad (3.5)$$

We now assume that the viscosity of the plasma depends only on the *orientation* of the magnetic field lines and not on the directions they *point* in. In other words, we assume, based on considerations described earlier, that the viscosity is invariant under inversion of the magnetic field direction  $\mathbf{b} \rightarrow -\mathbf{b}$ . Consequently, as far as the probability density function is concerned,  $\mathbf{t}$  is ‘headless’ and  $f_{\mathbf{x}}(\mathbf{t}) = f_{\mathbf{x}}(-\mathbf{t})$ . Because of this property, the first moment of the distribution  $f_{\mathbf{x}}$  is zero.

The second moment of the distribution is the variance tensor

$$\mathbf{M} = \frac{1}{4\pi} \int_{\mathbb{S}^2} f_{\mathbf{x}}(\mathbf{t}) \mathbf{t} \otimes \mathbf{t} d\omega. \quad (3.6)$$

Introducing an orthonormal basis  $\mathcal{B} = \{\mathbf{e}_1, \mathbf{e}_2, \mathbf{e}_3\}$ , the variance tensor can be written in the compact form

$$\mathbf{M} = \sum_{i,j=1}^3 \alpha_{ij} \mathbf{e}_i \otimes \mathbf{e}_j, \quad (3.7)$$

where

$$\alpha_{ij} = \frac{1}{4\pi} \int_{\mathbb{S}^2} f_{\mathbf{x}}(\mathbf{t}) t_i t_j d\omega, \quad (3.8)$$

( $t_1, t_2, t_3$ ) being the components of  $\mathbf{t}$  with respect to  $\mathcal{B}$ .

To make progress with the form of the structure tensor, we choose, without loss of generality,  $\mathbf{e}_3 = \mathbf{b}$ , and characterize  $\mathbf{t}$  in terms of the two Euler angles  $\theta \in [0, \pi]$  and  $\phi \in [0, 2\pi)$ :

$$\mathbf{t} = \sin \theta \cos \phi \mathbf{e}_1 + \sin \theta \sin \phi \mathbf{e}_2 + \cos \theta \mathbf{e}_3. \quad (3.9)$$

Because of the arbitrariness of the basis vectors  $\mathbf{e}_1$  and  $\mathbf{e}_2$ , we assume that the orientation density function is independent of  $\phi$ , i.e.

$$f_{\mathbf{x}}[\mathbf{t}(\theta, \phi)] = f_{\mathbf{x}}[\mathbf{t}(\theta)]. \quad (3.10)$$

Consequently, the normalization condition (3.5) becomes

$$\frac{1}{2} \int_0^\pi f_{\mathbf{x}}(\theta) \sin \theta d\theta = 1, \quad (3.11)$$

the off-diagonal terms of  $\mathbf{M}$  vanish and the diagonal terms remaining are, on use of the normalization condition, given by

$$\alpha_{11} = \alpha_{22} = \kappa, \quad \alpha_{33} = 1 - 2\kappa, \quad \kappa = \frac{1}{4} \int_0^\pi f_{\mathbf{x}}(\theta) \sin^3 \theta d\theta. \quad (3.12)$$

Thus, the variance tensor can be written in the compact form

$$\mathbf{M} = \kappa(\mathbf{e}_1 \otimes \mathbf{e}_1 + \mathbf{e}_2 \otimes \mathbf{e}_2) + (1 - 2\kappa)\mathbf{b} \otimes \mathbf{b} = \kappa \mathbf{I} + (1 - 3\kappa)\mathbf{b} \otimes \mathbf{b}. \quad (3.13)$$

The parameter  $\kappa$ , defined through equation (3.12)<sub>3</sub>, is called the *dispersion parameter* and represents the degree of anisotropy. Furthermore, since  $\mathbf{M}$  is positive semi-definite, the dispersion parameter must satisfy the inequalities

$$0 \leq \kappa \leq \frac{1}{2}. \quad (3.14)$$

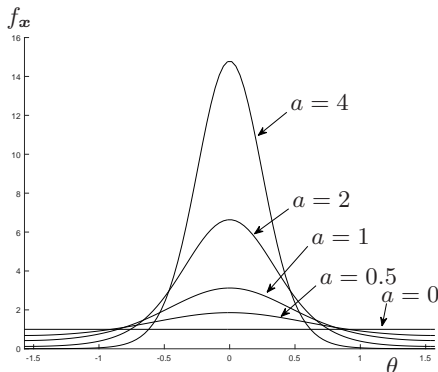


FIGURE 1. Modified Von Mises distribution for various values of the concentration parameter.

The perfect alignment of momentum transport through  $\mathbf{x}$  along the magnetic field is attained for  $\kappa = 0$ , whereas for  $\kappa = 1/3$  there is no preferred alignment and all orientations are equiprobable. For  $\kappa = 1/2$ , instead, the momentum transport through  $\mathbf{x}$  orients perpendicularly to the magnetic field and all the directions orthogonal to  $\mathbf{b}$  are equiprobable. However, since the magnetic field direction is the preferred direction, we require that the probability that the momentum transport through  $\mathbf{x}$  orients along  $\mathbf{b}$  is greater or equal to the probability that it orients along a direction perpendicular to the magnetic field. Therefore,  $1 - 2\kappa \geq \kappa$  and, in the light of (3.14), we shall limit our analysis to the interval

$$0 \leq \kappa \leq \frac{1}{3}. \quad (3.15)$$

In order to discuss the dispersion parameter  $\kappa$  we consider a transversely isotropic and  $\pi$ -periodic von Mises distribution. More precisely, we modify the standard  $\pi$ -periodic von Mises distribution to satisfy the normalization condition (3.11), giving

$$f_{\mathbf{x}}(\theta) = 2\sqrt{\frac{2a}{\pi}} \frac{\exp(2a \cos^2 \theta)}{\operatorname{erfi}(\sqrt{2a})}, \quad (3.16)$$

where  $\operatorname{erfi}(x) = -i\operatorname{erf}(ix)$  is the imaginary error function and  $a$  is a positive quantity called the *concentration parameter*. The orientation density function (3.16), used also by Gasser, Ogden & Holzapfel (2006) to model collagen fibre distributions in arteries, can be interpreted as the normal distribution projected onto the unit sphere. The modified Von Mises distribution (3.16) tends uniformly to the uniform distribution  $f_{\mathbf{x}} \equiv 1$  as  $a \rightarrow 0$ , while it tends to the Dirac delta  $\delta_0(\theta)$  centered at  $\theta = 0$  as  $a \rightarrow +\infty$  (figure 1). Therefore, this distribution gives the required directional behaviour for momentum transport when  $|\mathbf{B}|$  is weak or strong.

Inserting (3.16) into (3.12)<sub>3</sub> results, after integration, in an analytical expression for the dispersion parameter,

$$\kappa = \frac{1}{2} \left( 1 + \frac{1}{4a} \right) - \frac{\exp(2a)}{2\sqrt{2\pi a} \operatorname{erfi}(\sqrt{2a})}, \quad (3.17)$$

from which we deduce that the dispersion parameter decreases as  $a$  increases, tends to 0 as  $a \rightarrow +\infty$ , and  $\kappa \rightarrow 1/3$  as  $a \rightarrow 0$  (figure 2(a)). As a consequence, the momentum transport through  $\mathbf{x}$  can orient along any direction with the same probability as  $a \rightarrow 0$ , whereas it tends to align perfectly along the magnetic field for a very large concentration parameter.

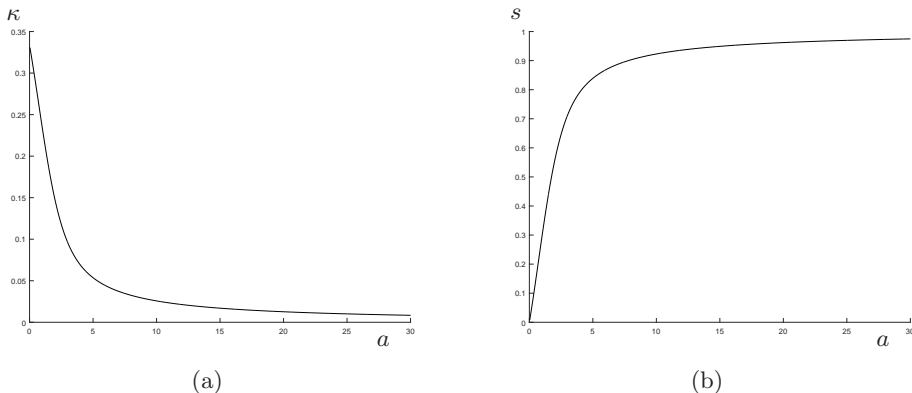


FIGURE 2. Dispersion and order parameter vs. concentration parameter.

Later it will be convenient to work with the traceless part of the variance tensor  $\mathbf{M}$ ,

$$\mathbf{H} = \mathbf{M} - \frac{1}{3}\mathbf{I} = s \left( \mathbf{b} \otimes \mathbf{b} - \frac{1}{3}\mathbf{I} \right), \quad s = 1 - 3\kappa. \quad (3.18)$$

Readers familiar with liquid crystal theory will recognise  $\mathbf{H}$  as similar to the order tensor for nematics (e.g. Napoli & Vergori 2012). Here, instead, in line with the nomenclature adopted in the theory of nonlinear anisotropic elasticity, we call  $\mathbf{H}$  the structure tensor. In view of (3.15), the *order parameter*  $s$  lies in the interval  $[0, 1]$ . Thus, the orientation of momentum transport through  $\mathbf{x}$  aligns perfectly along the magnetic field direction for  $s = 1$ , while it has no preferred direction for  $s = 0$ . Asymptotically, we have

$$s \sim \frac{4}{15}a + O(a^2) \quad \text{as } a \rightarrow 0, \quad (3.19)$$

and  $s \rightarrow 1$  as  $a \rightarrow +\infty$  (figure 2(b)).

If the viscous stress tensor  $\boldsymbol{\sigma}_V$  is to be applicable to magnetic fields of arbitrary topology, the order parameter  $s$  must represent some measure of the magnetic field strength. If a magnetic field contains a null point, where  $\mathbf{B} = \mathbf{0}$ , any anisotropic effect must ‘switch off’, with viscosity reverting to an isotropic form. In order to determine a constitutive function for  $s$  relating the order parameter to the magnetic field strength, we assume that the (non-dimensional) concentration parameter  $a$  depends on  $|\mathbf{B}|$ ,

$$a = \hat{a}(|\mathbf{B}|). \quad (3.20)$$

Since

- the probability that momentum transport orients along the magnetic field lines increases as the magnetic field strength increases,
- the momentum transport tends to orient perfectly along the magnetic field lines if the magnetic field is strong enough,
- the momentum transport tends to have no preferred direction for weak (or zero) magnetic fields,

we require that the constitutive function  $\hat{a}$  satisfies the following properties:

- (i)  $\hat{a}$  is a non-negative increasing function of  $|\mathbf{B}|$ ,
- (ii)  $\hat{a}(|\mathbf{B}|) \rightarrow +\infty$  as  $|\mathbf{B}| \rightarrow +\infty$ ,

$$(iii) \lim_{\mathbf{B} \rightarrow \mathbf{0}} \frac{\hat{a}(|\mathbf{B}|)}{|\mathbf{B}|^2} \in \mathbb{R}.$$

Property (iii) requires that the constitutive function for the concentration parameter is an infinitesimal in the magnetic field strength of order greater than or equal to 2. The reason of this requirement will be clear in few lines.

From (3.18) and the definition of  $\mathbf{b}$ , the structure tensor  $\mathbf{H}$  can be re-written as

$$\mathbf{H} = \frac{\hat{s}(|\mathbf{B}|)}{|\mathbf{B}|^2} \left( \mathbf{B} \otimes \mathbf{B} - \frac{|\mathbf{B}|^2}{3} \mathbf{I} \right), \quad (3.21)$$

where, in view of (3.17) and (3.20),

$$s = \hat{s}(|\mathbf{B}|) = \frac{3 \exp[2\hat{a}(|\mathbf{B}|)]}{2\sqrt{2\pi\hat{a}(|\mathbf{B}|)} \operatorname{erfi}[\sqrt{2\hat{a}(|\mathbf{B}|)}]} - \frac{1}{2} \left[ 1 + \frac{3}{4\hat{a}(|\mathbf{B}|)} \right]. \quad (3.22)$$

Finally, thanks to (3.19) and property (iii), we can define the structure tensor also at points where the magnetic field vanishes, i.e. equation (3.21) applies to arbitrary magnetic topologies. The simplest (non-trivial) form for the concentration parameter that satisfies conditions (i-iii) is  $a = a_0 |\mathbf{B}|^2$ , for some constant  $a_0 > 0$ .

### 3.3. Viscosity tensor

Now that a suitable form for the structure tensor  $\mathbf{H}$  has been developed, we can focus on what kind of expression the viscous stress tensor of equation (3.4) can take. The constitutive equation for  $\boldsymbol{\sigma}_V$  (3.4) must be objective (that is, invariant to a change of observer) and hence satisfy the identity

$$\hat{\boldsymbol{\sigma}}_V(\mathbf{Q}\mathbf{D}\mathbf{Q}^T, \mathbf{Q}\mathbf{H}\mathbf{Q}^T, |\mathbf{Q}\mathbf{B}|) = \mathbf{Q}\hat{\boldsymbol{\sigma}}_V(\mathbf{D}, \mathbf{H}, |\mathbf{B}|)\mathbf{Q}^T, \quad (3.23)$$

for all proper orthogonal tensors  $\mathbf{Q}$ . Following Ericksen (1960), Spencer (1971) and Dorfmann, Ogden & Wineman (2007), and noting that

$$\mathbf{H}^n = \frac{\hat{s}^{n-1}(|\mathbf{B}|)}{3} \mathbf{H} + \frac{2\hat{s}^n(|\mathbf{B}|)}{3^n} \mathbf{I}, \quad \operatorname{tr}(\mathbf{H}^n) = \frac{2\hat{s}^n(|\mathbf{B}|)}{3^{n-1}} \quad (n = 2, 3), \quad (3.24)$$

we can write down the most general constitutive relation for  $\boldsymbol{\sigma}_V$  satisfying equation (3.23):

$$\boldsymbol{\sigma}_V = \alpha_0 \mathbf{I} + \alpha_1 \mathbf{D} + \alpha_2 \mathbf{D}^2 + \alpha_3 \mathbf{H} + \alpha_4 (\mathbf{D}\mathbf{H} + \mathbf{H}\mathbf{D}) + \alpha_5 (\mathbf{D}^2 \mathbf{H} + \mathbf{H}\mathbf{D}^2), \quad (3.25)$$

which, as required by the balance of angular momentum, is symmetric. The six viscosity coefficients  $\alpha_i$  ( $i = 0, \dots, 5$ ) are functions of  $|\mathbf{B}|$  and the integrity basis of the two tensors  $\mathbf{D}$  and  $\mathbf{H}$ . In view of (3.24), the integrity basis for the current problem consists of the following five invariants

$$\operatorname{tr}(\mathbf{D}), \operatorname{tr}(\mathbf{D}^2), \operatorname{tr}(\mathbf{D}^3), \operatorname{tr}(\mathbf{D}\mathbf{H}), \operatorname{tr}(\mathbf{D}^2 \mathbf{H}). \quad (3.26)$$

This is a minimal set of invariants since the trace of the product of two second-order Cartesian tensors is equal to the trace of the tensor product with the factors written in reverse (Spencer 1971). The first three invariants in (3.26) account for the dependence on the strain rate tensor  $\mathbf{D}$ ; the remaining two invariants account for the interaction of the deformation rate and the structure tensor and are sometimes referred to as pseudo-invariants (Holzapfel 2000).

Taking into account (2.7), the viscous stress tensor  $\boldsymbol{\sigma}_V$  can be written as

$$\begin{aligned} \boldsymbol{\sigma}_V &= -p_d \mathbf{I} + \overset{\circ}{\boldsymbol{\sigma}}_V = -p_d \mathbf{I} + \beta_1 \mathbf{W} + \beta_2 \left[ \mathbf{W}^2 - \frac{1}{3} \text{tr}(\mathbf{W}^2) \mathbf{I} \right] \\ &+ \beta_3 \mathbf{H} + \beta_4 \left[ \mathbf{WH} + \mathbf{HW} - \frac{2}{3} \text{tr}(\mathbf{WH}) \mathbf{I} \right] \\ &+ \beta_5 \left[ \mathbf{W}^2 \mathbf{H} + \mathbf{HW}^2 - \frac{2}{3} \text{tr}(\mathbf{W}^2 \mathbf{H}) \mathbf{I} \right] \end{aligned} \quad (3.27)$$

where

$$p_d = - \left[ \alpha_0 + \frac{\alpha_1}{3} \text{tr}(\mathbf{D}) + \frac{\alpha_2}{3} \text{tr}(\mathbf{D}^2) + \frac{2\alpha_4}{3} \text{tr}(\mathbf{DH}) + \frac{2\alpha_5}{3} \text{tr}(\mathbf{D}^2 \mathbf{H}) \right],$$

is the hydrodynamic pressure, and

$$\begin{aligned} \beta_1 &= \frac{\alpha_1}{2} + \frac{\alpha_2}{3} \text{tr}(\mathbf{D}), & \beta_2 &= \frac{\alpha_2}{4}, & \beta_3 &= \alpha_3 + \frac{2}{3} \text{tr}(\mathbf{D}) \left[ \alpha_4 + \frac{\alpha_5}{3} \text{tr}(\mathbf{D}) \right], \\ \beta_4 &= \frac{\alpha_4}{2} + \frac{\alpha_5}{3} \text{tr}(\mathbf{D}), & \beta_5 &= \frac{\alpha_5}{4}. \end{aligned} \quad (3.28)$$

Obviously,  $\overset{\circ}{\boldsymbol{\sigma}}_V$  is traceless. Then, from equations (3.1) and (3.27), the full stress tensor becomes

$$\boldsymbol{\sigma}_V = -p \mathbf{I} + \boldsymbol{\sigma}_M + \overset{\circ}{\boldsymbol{\sigma}}_V, \quad (3.29)$$

where  $p = p_s + p_d$  is the plasma pressure.  $\overset{\circ}{\boldsymbol{\sigma}}_V$  represents the most general form of the viscous stress tensor in our model. There are many possible specializations and we shall now consider two.

### 3.4. Model 1: single-fluid Braginskii

As mentioned previously, the single-fluid Braginskii tensor (2.17) is a special case of  $\overset{\circ}{\boldsymbol{\sigma}}_V$ . This is easily shown by setting

$$\beta_1 = \frac{2\eta_2(|\mathbf{B}|) + \eta_1(|\mathbf{B}|)}{3}, \quad (3.30)$$

$$\beta_3 = \frac{3\eta_0 + \eta_1(|\mathbf{B}|) - 4\eta_2(|\mathbf{B}|)}{\hat{s}^2(|\mathbf{B}|)} \text{tr}(\mathbf{DH}), \quad (3.31)$$

$$\beta_4 = \frac{\eta_2(|\mathbf{B}|) - \eta_1(|\mathbf{B}|)}{\hat{s}(|\mathbf{B}|)}, \quad (3.32)$$

with  $\eta_0$  constant,  $\eta_1$  and  $\eta_2$  as in (2.14), and the remaining  $\beta$ 's to zero. A family of Braginskii-like viscosity coefficients can be found by first specifying the correct asymptotic behaviour of  $\beta_1$ ,  $\beta_3$  and  $\beta_4$ , i.e. the viscosity tensor produces parallel viscosity in the strong-field limit and isotropic viscosity in the weak-field limit. We shall not pursue this approach here but, instead, consider a simplified model that could be useful in large-scale coronal simulations.

### 3.5. Model 2: parallel-isotropic switch

Most of the work concerning Braginskii MHD that we have cited in this paper has focussed on the strong-field limit. We have also highlighted that this regime applies almost everywhere in the solar corona. For simulations of large-scale coronal phenomena, where null points exist at isolated locations throughout the domain (and are perhaps spread over only a few grid points), the effects of the full Braginskii tensor may not be

adequately resolved. Instead, a simpler model where the direct switch between parallel and isotropic viscosity can be controlled may prove more useful. At null points, the parallel viscosity cannot be separated from the perpendicular viscosity in the limit as  $|\mathbf{B}| \rightarrow 0$  in the Braginskii tensor (2.17). In equation (3.27), however, we can choose the coefficients depending on our requirements. Setting

$$\begin{aligned}\beta_1 &= \eta_0[1 - \hat{s}^2(|\mathbf{B}|)], \\ \beta_3 &= 3\eta_0 \text{tr}(\mathbf{DH}), \\ \beta_i &= 0 \quad (i = 2, 4, 5),\end{aligned}\tag{3.33}$$

where  $\eta_0$  is the viscosity in an unmagnetized plasma, gives the parallel viscosity (2.12) in the strong-field limit regime and isotropic viscosity when the field goes to zero. The viscous stress tensor can be written as

$$\overset{\circ}{\boldsymbol{\sigma}}_V = \eta_0[1 - \hat{s}^2(|\mathbf{B}|)]\mathbf{W} + \frac{3}{2}\eta_0 \frac{\hat{s}^2(|\mathbf{B}|)}{|\mathbf{B}|^4}(\mathbf{W}\mathbf{B} \cdot \mathbf{B}) \left( \mathbf{B} \otimes \mathbf{B} - \frac{|\mathbf{B}|^2}{3}\mathbf{I} \right).\tag{3.34}$$

Equation (3.34) represents an improvement on current coronal models that only consider isotropic viscosity. It also represents a simple extension of the many models that have only parallel viscosity. Later, we shall demonstrate that the ‘region of switching’ from parallel to isotropic viscosity can be controlled using the concentration parameter  $\hat{a}$ .

#### 4. Illustrative application

In this section we apply the anisotropic models of the viscous tensor (equations 2.17 and 3.34) to the deformation of a magnetic null point. Our purpose here is not to study a particular phenomenon but to highlight the practicalities of implementing the two anisotropic models. We also demonstrate that, even with mild driving velocities, the viscosity in a non-trivial topology can behave significantly differently if the tensor is anisotropic rather than isotropic. We shall consider three cases: isotropic viscosity only, Braginskii viscosity and the parallel-isotropic model. For each case we will study the role of viscous heating and how it is distributed throughout the domain. In these simulations, we solve the compressible resistive MHD equations using a Lagrangian remap scheme (Arber et al. 2001). In nondimensional form, these equations are

$$\frac{D\rho}{Dt} = -\rho \nabla \cdot \mathbf{u},\tag{4.1}$$

$$\frac{D\mathbf{u}}{Dt} = -\frac{1}{\rho} \nabla p + \frac{1}{\rho} (\nabla \times \mathbf{B}) \times \mathbf{B} + \frac{1}{\rho} \nabla \cdot \boldsymbol{\sigma}_V,\tag{4.2}$$

$$\frac{D\mathbf{B}}{Dt} = (\mathbf{B} \cdot \nabla)\mathbf{u} - (\nabla \cdot \mathbf{u})\mathbf{B} + \tilde{\eta} \nabla^2 \mathbf{B},\tag{4.3}$$

$$\frac{D\varepsilon}{Dt} = -\frac{p}{\rho} \nabla \cdot \mathbf{u} + \frac{1}{\rho} \boldsymbol{\sigma}_V : \nabla \mathbf{u} + \frac{\tilde{\eta}}{\rho} |\nabla \times \mathbf{B}|^2,\tag{4.4}$$

with specific energy density

$$\varepsilon = \frac{p}{(\gamma - 1)\rho},\tag{4.5}$$

where  $\rho$  is the plasma density and the specific heat ratio  $\gamma = 5/3$ . The material derivative is

$$\frac{D(\cdot)}{Dt} = \frac{\partial(\cdot)}{\partial t} + \mathbf{u} \cdot \nabla(\cdot).\tag{4.6}$$

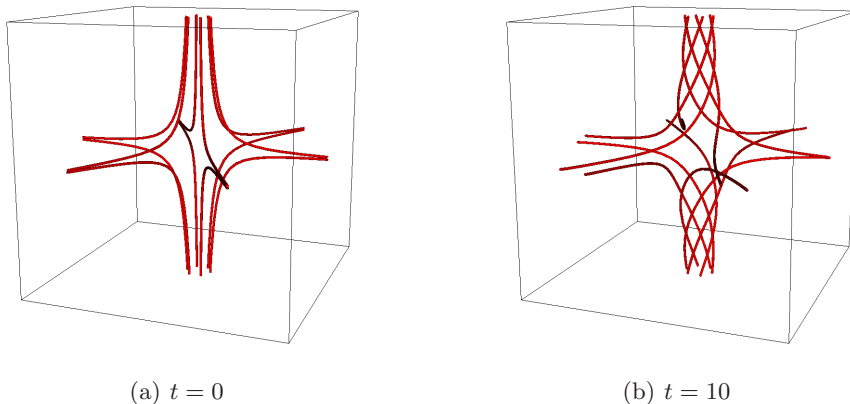


FIGURE 3. Selected magnetic field lines.

Equations (4.1)-(4.5) are nondimensionalized with respect to a reference magnetic field strength  $|\mathbf{B}_r|$ , length  $L_r$  and density  $\rho_r$ . For our applications these are arbitrary.  $\tilde{\eta}$  is the (dimensionless) resistivity and we choose its value to be  $10^{-4}$ . In the following applications we shall select the (dimensionless) parallel viscosity coefficient  $\eta_0 = 10^{-4}$ . When numerically implementing  $\hat{s}^2(|\mathbf{B}|)$  from equation (3.22) with  $\hat{a}(|\mathbf{B}|) = a_0|\mathbf{B}|^2$ , we use a cubic spline approximation with natural boundary conditions. This is much simpler, faster and more accurate than implementing series expansions for the imaginary error function.

We consider a domain with dimensions of  $[-3,3]^3$  and a mesh size of  $500^3$ . The magnetic field has the form

$$\mathbf{B} = \frac{B_0}{l_0}(x, y, -2z)^T, \quad (4.7)$$

where  $B_0 = l_0 = 1$ . The resolution we have chosen is far higher than typical simulations of null points. The boundaries are closed in all three directions, as in other null point studies (e.g. Pontin, Bhattacharjee & Galsgaard 2007; Galsgaard & Pontin 2011). On the upper and lower boundaries we impose twisting motions. On the lower boundary we have

$$\mathbf{u} = \frac{v_0}{2l_0} \left[ 1 + \tanh \left( 2 \frac{t - t_0}{t_d} \right) \right] \mathbf{u}_h, \quad (4.8)$$

with  $\mathbf{u}_h = (u'_x, u'_y, 0)^T$  and

$$u'_x = \begin{cases} -\pi y \frac{\sin(\pi r)}{r} & \text{if } r^2 < 1, \\ 0 & \text{if } r^2 \geq 1, \end{cases} \quad u'_y = \begin{cases} \pi x \frac{\sin(\pi r)}{r} & \text{if } r^2 < 1, \\ 0 & \text{if } r^2 \geq 1, \end{cases} \quad (4.9)$$

where  $r^2 = x^2 + y^2$ . The velocity driver on the top boundary is the same as in equations (4.8) and (4.9) except that it moves in the opposite direction. The sub-Alfvénic driving velocity is  $v_0 = 0.05$  and  $l_0$  and  $t_d$  are parameters which are both set to 1. The time when boundary velocity has been smoothly ramped to about  $v_0/2$  is  $t_0 = 2$ . The effect of these boundary motions is to twist the magnetic field and generate gradients in both the magnetic field and the velocity of the plasma.

To illustrate the geometry of the magnetic field lines, figure 3 displays the field at the initial condition  $t = 0$  and after substantial deformation at  $t = 10$ .

Note that parts (a) and (b) in figure 3 do not necessarily display the same field lines.

#### 4.1. Concentration parameter

For the parallel-isotropic model, we are required to choose a form for the nondimensional concentration parameter  $\hat{a}$ . As mentioned earlier we assume that  $\hat{a} = a_0|\mathbf{B}|^2$ . In order to make a simple comparison between the different models, we shall choose  $a_0 = \alpha^2$  so that  $\hat{a} = x_i^2$ . For this particular numerical experiment, we set  $\alpha|\mathbf{B}_r| = 6$ . This choice allows for a simple comparison between the models and for the different heating contributions to be easily visualized. In the Discussion at the end of the paper, we shall return to the consequences of choosing different expressions for  $\hat{a}$  and  $x_i$ .

#### 4.2. Heating profiles

We shall now examine how the different viscosity models heat the plasma. The viscous heating in the fully isotropic model is

$$Q^{\text{iso}} = \boldsymbol{\sigma}_V^{\text{iso}} : \nabla \mathbf{u} = \frac{\eta_0}{2} \text{tr}(\mathbf{W}^2). \quad (4.10)$$

In the Braginskii model, the heating terms from the isotropic and anisotropic parts are

$$Q_1^{\text{iso}} = \frac{\eta_1}{2} \text{tr}(\mathbf{W}^2), \quad (4.11)$$

$$Q_1^{\text{ani}} = \frac{3\eta_0 + \eta_1 - 4\eta_2}{4|\mathbf{B}|^4} (\mathbf{W}\mathbf{B} \cdot \mathbf{B})^2 + \frac{\eta_2 - \eta_1}{|\mathbf{B}|^2} |\mathbf{W}\mathbf{B}|^2. \quad (4.12)$$

In the parallel-isotropic model, the heating terms from the isotropic and anisotropic parts are

$$Q_2^{\text{iso}} = \frac{\eta_0}{2} [1 - \hat{s}^2(|\mathbf{B}|)] \text{tr}(\mathbf{W}^2), \quad (4.13)$$

$$Q_2^{\text{ani}} = \frac{3\eta_0 \hat{s}^2(|\mathbf{B}|)}{4|\mathbf{B}|^4} (\mathbf{W}\mathbf{B} \cdot \mathbf{B})^2. \quad (4.14)$$

From (2.14) and (4.11)–(4.14) we deduce that, at null points, the total viscous heating in both models ( $i = 1, 2$ ) equals the viscous heating in the fully isotropic model, specifically

$$Q_i^{\text{iso}} + Q_i^{\text{ani}} \rightarrow Q^{\text{iso}} \quad \text{as } |\mathbf{B}| \rightarrow 0 \quad (i = 1, 2), \quad (4.15)$$

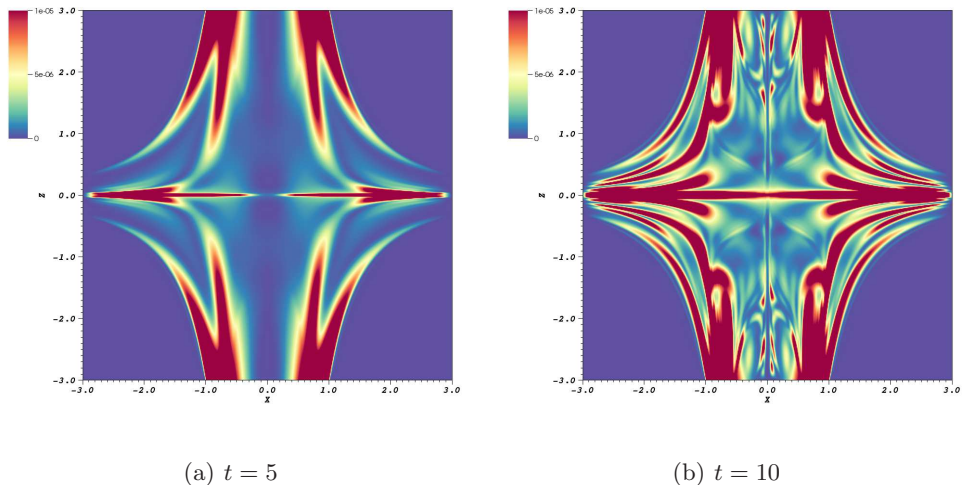
while in the limit of strong magnetic field we have

$$Q_i^{\text{iso}} + Q_i^{\text{ani}} \approx \frac{3}{4} \eta_0 (\mathbf{W}\mathbf{b} \cdot \mathbf{b})^2 \quad (i = 1, 2). \quad (4.16)$$

That is, the parallel-isotropic model reproduces the asymptotic limits of the full Braginskii model.

Figure 4 displays slices of  $Q^{\text{iso}}$  in the  $y = 0$  plane at two different times.

As the motions on the upper and lower boundaries continue to be driven, torsional waves are transmitted towards the null point. Initially, the waves follow the path of the *spine*, a vertical line through the null point. As the field lines then splay out into the *fan*, a plane through the null orthogonal to the spine, the plasma follows the magnetic field. In the fully isotropic model, viscous heating occurs on the fan plane and in vertical locations near the spine. As time increases, more of the domain becomes heated by viscosity. By comparison, the viscous heating due to the isotropic parts ( $Q_1^{\text{iso}}$  and  $Q_2^{\text{iso}}$ ) of the other models exhibits different behaviour. Their profiles are displayed in figure 5.

FIGURE 4.  $Q^{\text{iso}}$  slices in the  $y = 0$  plane.

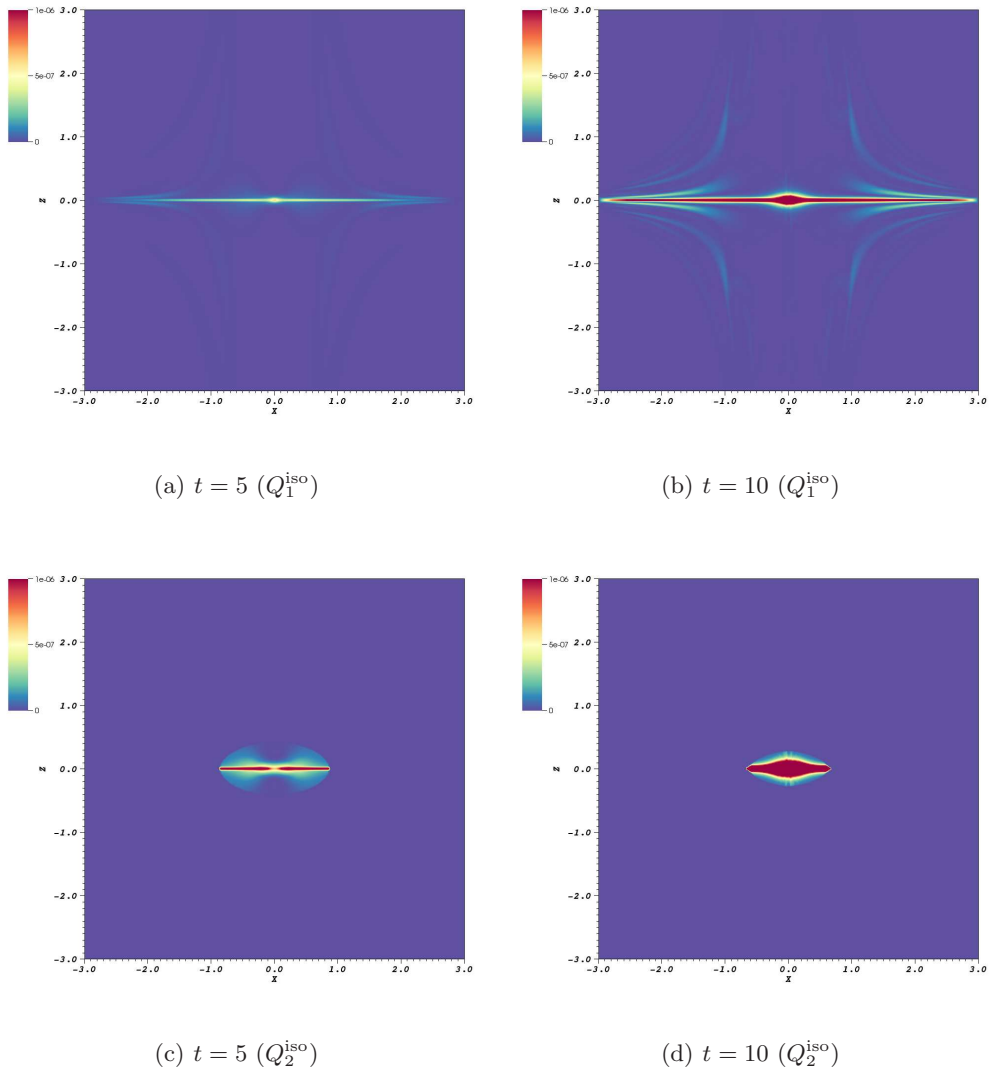
Note that the magnitude of heating shown on the colour bar in figure 5 is an order of magnitude less than that of figure 4 in order to reveal structure. Considering the Braginskii model first (figures 5(a) and 5(b)), viscous heating is almost entirely confined to the fan plane. This behaviour is to be expected as the imposed twisting motions generate a shear layer in the fan plane. Unlike the fully isotropic model, however, the heating does not spread significantly beyond the fan plane. The viscous heating of the parallel-isotropic model (figures 5(c) and 5(d)) is also concentrated on the fan plane but is truncated compared to the Braginskii model.

Figure 6 displays slices of viscous heating due to the anisotropic parts ( $Q_1^{\text{ani}}$  and  $Q_2^{\text{ani}}$ ) of the models at  $t=5, 10$ .

Comparing figures of the Braginskii model, 6(a) and 6(b), and the parallel-isotropic model, 6(c) and 6(d), the viscous heating profiles have many similarities. The main differences occur close to the null point. At  $t = 5$ , the heating due to the Braginskii model contains small-scale structures very close to the null point, see figure 6(a). The parallel-isotropic model does not include these small-scale structures, see figure 6(c). Away from the null point, both heating profiles are very similar. This is to be expected from equation (4.16).

Later, at  $t = 10$ , the anisotropic heating from the Braginskii model has spread to the null point itself, see figure 6(b). The parallel-isotropic model produces a very similar heating profile but now there is no anisotropic heating at the null point, see figure 6(d).

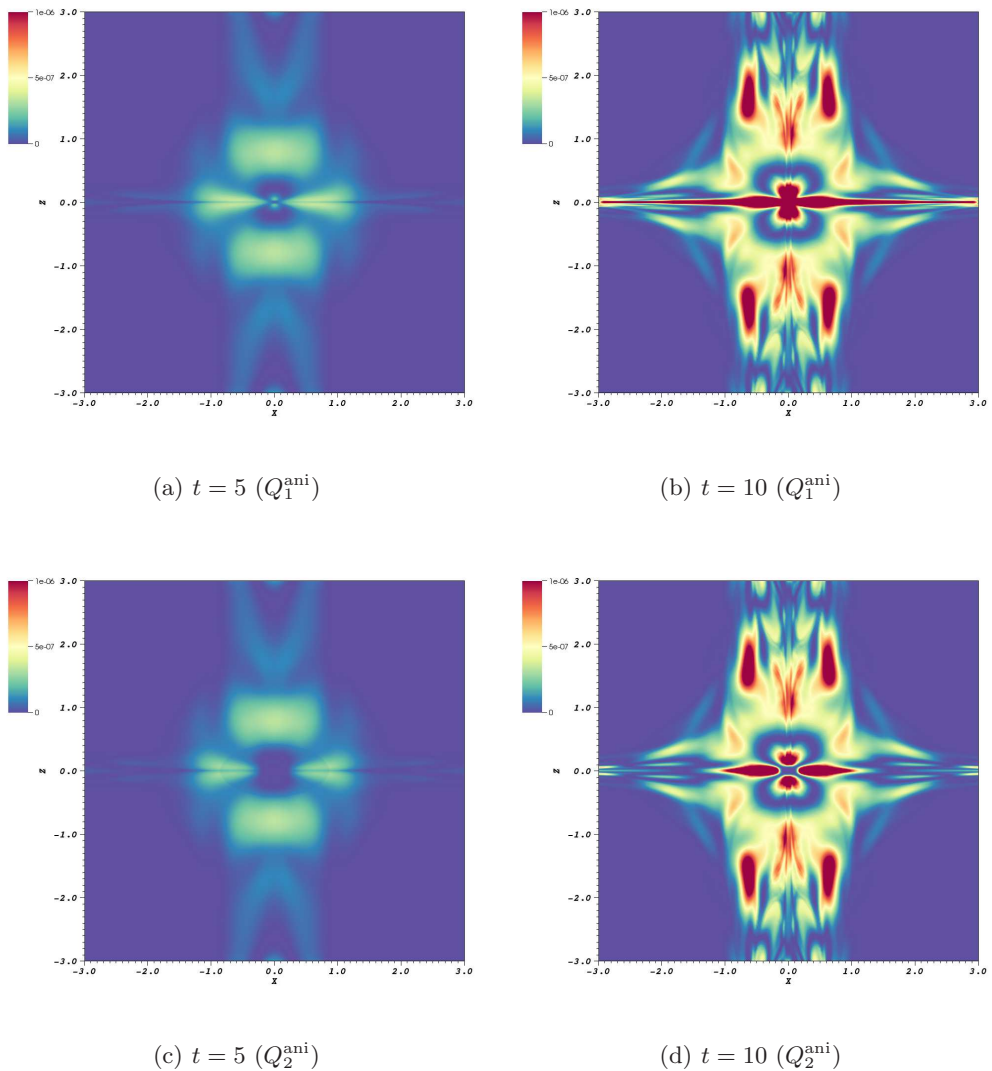
Comparing the heating profiles of the anisotropic models, figures 5 and 6, to the fully isotropic model, figure 4, reveals significant differences in the magnitude of the heating and its spatial distribution. Throughout large parts of the magnetic field, including both the spine and fan, isotropic viscous heating is an order of magnitude greater than the heating from both the anisotropic models.

FIGURE 5.  $Q_1^{\text{iso}}$  and  $Q_2^{\text{iso}}$  slices in the  $y = 0$  plane.

## 5. Discussion

### 5.1. Summary

In this paper, we investigate single-fluid MHD with anisotropic viscosity, particularly for applications to the solar corona. We begin with the classic Braginskii model (Braginskii 1965) of anisotropic viscosity in a plasma. MHD with the Braginskii viscous model is often referred to as Braginskii MHD. The majority of applications of Braginskii MHD consider the strong-field limit, where viscosity parallel to the magnetic field dominates. The majority of the solar coronal magnetic field is in this strong-field limit. The exceptions occur when the field strength reduces to zero, e.g. at null points. Such locations are linked to the complex magnetic topology of the solar corona and play important roles in many eruptive phenomena, such as flares and coronal mass ejections (e.g. Priest 2014). In order to have a consistent viscosity model, the viscous stress tensor

FIGURE 6.  $Q_1^{\text{ani}}$  and  $Q_2^{\text{ani}}$  slices in the  $y = 0$  plane.

has to switch from the parallel form to the standard isotropic form when  $|\mathbf{B}| = 0$ . The Braginskii viscous tensor achieves this but some care is required to show that the tensor possesses the correct asymptotic behaviour as  $|\mathbf{B}| \rightarrow 0$ . By combining the five standard Braginskii viscous stress tensors, as given in equation (2.2), together, it can be shown that the tensor has the correct asymptotic behaviour in the weak-field limit. This ‘combined form’ is also the recommended way of implementing the full Braginskii tensor in simulations in order to avoid numerical errors due to terms that are no longer defined, e.g.  $\eta_0 \mathbf{W}^{(0)}$  when  $|\mathbf{B}| = 0$ .

Above we mentioned that all five of the Braginskii tensors can be combined to provide expressions that are suitable for arbitrary magnetic topologies. However, in this paper, we have only considered the first three tensors. We have dropped  $\eta_3 \mathbf{W}^{(3)}$  and  $\eta_4 \mathbf{W}^{(4)}$  as their effects are marginal in many coronal applications (e.g. Hollweg 1985; Bogaert & Goossens

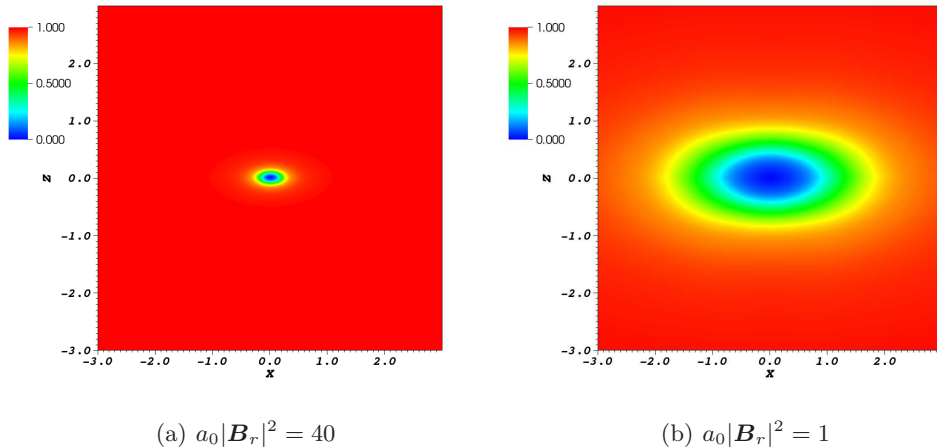


FIGURE 7. Slices of  $\hat{s}$  for different values of  $a_0|\mathbf{B}_r|^2$  at  $t = 5$  in the  $y = 0$  plane.

1991). We do not also drop the perpendicular contribution since, as mentioned above, these terms are required to be written in a combined form with the parallel viscosity. For applications which require the drift terms, the combination of the drift tensors required to satisfy the weak-field limit is presented in the Appendix.

The remaining terms in the Braginskii model represent parallel, perpendicular and isotropic viscosity. We show that these viscosities have a clear interpretation at the single-fluid continuum level in terms of the distribution of momentum transport. As the field becomes stronger, momentum transport aligns itself with the orientation of the field. When the field is zero, there is no preferred direction. We find the most general traceless viscous stress tensor that satisfies these conditions. The Braginskii model is shown to be a specialization of this general model. Another model is also considered which represents a direct switch from parallel to isotropic viscosity.

The Braginskii and parallel-isotropic models are implemented in simulations of a deformed magnetic null point, alongside a purely isotropic viscous model. It is demonstrated that the fully isotropic model, that is usually adopted in coronal models, produces viscous heating that is an order of magnitude greater than the anisotropic models.

## 5.2. Practical aspects

Comparing figures 6(a) and 6(c), the heating patterns are very similar except near the null point. For this simple illustrative example, we have taken  $\alpha|\mathbf{B}_r| = 6$ . For a typical coronal model,  $\alpha|\mathbf{B}_r| \sim 10^4$  would not be unrealistic. Hence, the near-null viscous heating in the Braginskii model may not be resolved, especially if a null point only occupies a few grid points, leading to anisotropic heating at nulls. One practical solution for this would be to implement the parallel-isotropic model and use the concentration parameter  $\hat{a}$  to control the size of the isotropic heating domain. Depending on the application, the concentration parameter could be set to produce more or less isotropic heating. For example, consider the simple model  $\hat{a} = a_0|\mathbf{B}_r|^2$ . Figure 7 displays slices of  $\hat{s}$  for null point simulations with the parallel-isotropic model and different values of  $a_0$ . For large-scale models of the solar atmosphere, e.g. flux emergence (MacTaggart & Haynes 2014; MacTaggart et al. 2015), null points are important but are not likely to be adequately resolved to determine the fine-scale structure of the Braginskii model, as discussed above.

Here, the parallel-isotropic model, with the flexibility in determining the size of the ‘isotropic region’, could improve the current fully isotropic viscosity models.

### 5.3. Future work

As follow-up work to this paper, we aim to apply the discussed anisotropic viscosity models to a variety of applications in the solar corona. Several phenomena, e.g. the kink and tearing instabilities, are often considered to be mechanisms by which many small-scale reconnection events can heat the coronal plasma (e.g. Bowness et al. 2013; Bareford & Hood 2015; Tam et al. 2015; Hood et al. 2016). The work of Hollweg, Craig, Litvinenko and Armstrong, cited earlier, has suggested that the contribution of viscous heating can be as important as Ohmic heating in the solar corona. Our simple simulations of deformed null points highlight that there are large differences in viscous heating between isotropic and anisotropic models. We plan to investigate anisotropic effects in 3D kink-unstable configurations and tearing current sheets with applications to coronal heating.

We would like to thank the Carnegie Trust for a Research Incentive Grant (Ref: 70323). Computational resources were provided by the EPSRC funded ARCHIE-WeSt High Performance Computer ([www.archie-west.ac.uk](http://www.archie-west.ac.uk)), EPSRC grant no. EP/K000586/1. Jamie Quinn is supported by an EPSRC DTA studentship.

## Appendix A. The numerical implementation of the drift terms

Since the focus of this paper has been on viscous heating in the solar corona, we have ignored the drift terms  $\eta_3 \mathbf{W}^{(3)}$  and  $\eta_4 \mathbf{W}^{(4)}$  from the full Braginskii viscous tensor. However, for applications where these terms may be important, we can use the analysis from section 2.2 to write these tensors in a form suitable for simulations of arbitrary magnetic topologies. If  $\eta_3 \mathbf{W}^{(3)} + \eta_4 \mathbf{W}^{(4)}$  is written in equation (2.1) using the standard representations (2.5) and (2.6), it will contain terms that are undefined at null points. We, therefore, need to rearrange the tensors in the following form

$$\eta_3 \mathbf{W}^{(3)} + \eta_4 \mathbf{W}^{(4)} = \frac{\eta_3}{2} (\mathbf{Z}\mathbf{W} - \mathbf{W}\mathbf{Z}) + \left( \eta_4 - \frac{\eta_3}{2} \right) [(\mathbf{Z}\mathbf{W}\mathbf{b}) \otimes \mathbf{b} + \mathbf{b} \otimes (\mathbf{Z}\mathbf{W}\mathbf{b})]. \quad (\text{A } 1)$$

Before demonstrating that the terms in equation (A 1) are defined at null points, as done for  $\eta_1$  and  $\eta_2$ , we relabel the viscosity coefficients (2.9) as

$$\eta_4 = \frac{\eta_0 \alpha |\mathbf{B}| (\alpha^2 |\mathbf{B}|^2 + a_4)}{\alpha^4 |\mathbf{B}|^4 + a_3 \alpha^2 |\mathbf{B}|^2 + a_2}, \quad \eta_3 = \eta_4 (2|\mathbf{B}|), \quad (\text{A } 2)$$

where  $x_i = \alpha |\mathbf{B}|$ . As  $|\mathbf{B}| \rightarrow 0$ ,

$$\eta_3 \sim \eta_0 \left[ \frac{2a_4}{a_2} \alpha |\mathbf{B}| + 8 \left( \frac{1}{a_2} - \frac{a_3 a_4}{a_2^2} \right) \alpha^3 |\mathbf{B}|^3 \right] + O(|\mathbf{B}|^5), \quad (\text{A } 3)$$

$$\eta_4 \sim \eta_0 \left[ \frac{a_4}{a_2} \alpha |\mathbf{B}| + \left( \frac{1}{a_2} - \frac{a_3 a_4}{a_2^2} \right) \alpha^3 |\mathbf{B}|^3 \right] + O(|\mathbf{B}|^5). \quad (\text{A } 4)$$

Hence, it follows that

$$\eta_3 \sim O(|\mathbf{B}|) \quad \text{and} \quad \eta_4 - \frac{\eta_3}{2} \sim O(|\mathbf{B}|^3), \quad (\text{A } 5)$$

as  $|\mathbf{B}| \rightarrow 0$ , which are required for the tensors to be well-defined at null points.

## REFERENCES

- ARBER, T. D., LONGBOTTOM, A. W., GERRARD, C. L. & MILNE, A. M. 2001 A staggered grid, Lagrangian-Eulerian remap code for 3-D MHD simulations. *J. Comp. Phys.* **171** 151–181.
- ARMSTRONG, C. K., CRAIG, I. J. D. & LITVINENKO, Y. E. 2011 Viscous effects in time-dependent planar reconnection. *Astron. & Astrophys.* **534** A25.
- ARMSTRONG, C. K. & CRAIG, I. J. D. 2013 Visco-resistive dissipation in transient reconnection driven by the Orzag-Tang vortex. *Solar Phys.* **283** 463–471.
- ARMSTRONG, C. K. & CRAIG, I. J. D. 2014 Visco-resistive dissipation in strongly driven transient reconnection. *Solar Phys.* **289** 869–877.
- BALE, S. D., KASPER, J. C., HOWES, G. G., QUATAERT, E., SALEM, C. & SUNDKVIST, D. 2009 Magnetic fluctuation power near proton temperature anisotropy instability thresholds in the solar wind. *Phys. Rev. Lett.*, **103**, 211101
- BAREFORD, M. R. & HOOD, A. W. 2015 Shock heating in numerical simulations of kink-unstable coronal loops. *Phil. Trans. R. Soc. Lond. A.* **373** 20140266.
- BERLOK, T. & PESSAH, M. E. 2015 Plasma instabilities in the context of current helium sedimentation models: dynamical implications for the ICM in galaxy clusters. *Astrophys. J.* **813** 22.
- BISKAMP, D. 1993 Nonlinear magnetohydrodynamics. Cambridge Monographs on Plasma Physics, Cambridge University Press.
- BOGAERT, E., GOOSSENS, M 1991 The visco-resistive stability of arcades in the corona of the Sun. *Solar Phys.* **132** 109–124.
- BOWNESS, R., HOOD, A. W., PARNELL, C. E. 2013 Coronal heating and nonflares: current sheet formation and heating. *Astron. & Astrophys.* **560** A89.
- BRAGINSKII, S. I. 1965 Transport processes in a plasma. *Rev. Plasma Phys.* **1** 205–311.
- CHEW, G. F., GOLDBERGER, M. L. & LOW, F. E. 1956 The Boltzman equation and the one-fluid hydrodynamic equations in the absence of particle collisions *Proc. R. Soc. Lond. A.* **236** 112–118.
- CRAIG, I. J. D. 2010 Anisotropic viscous dissipation in transient reconnecting plasmas. *Astron. & Astrophys.* **515** A96.
- CRAIG, I. J. D. & LITVINENKO, Y. E. 2010 Energy losses by anisotropic viscous dissipation in transient magnetic reconnection. *Astrophys. J.* **725** 886–893.
- DORFMANN, A., OGDEN, R. W. & WINEMAN, A. S. 2007 A three-dimensional non-linear constitutive law for magnetorheological fluids, with applications. *Int. J. Non-Lin. Mech.* **42** 381–390.
- EPPERLEIN, E. M. & HAINES, M. G. 1986 Plasma transport coefficients in a magnetic field by direct numerical solution of the Fokker-Planck equation. *Phys. Plasmas* **29** 1029–1041.
- ERICKSEN, J. L. 1960 Transversely isotropic fluids. *Kolloid-Zeitschrift* **173** 117–122.
- GALSGAARD, K., & PONTIN, D. I. 2011 Steady state reconnection at a single 3D magnetic null point. *Astron. & Astrophys.* **529** A20.
- GASSER, T. C., OGDEN, R. W. & HOLZAPFEL, G. A. 2006 Hyperelastic modelling of arterial layers with distributed collagen fibre orientations. *J. R. Soc. Interface* **3** 15–35.
- HOGAN, J. T. 1984 Collisional transport of momentum in axisymmetric configurations. *Phys. Fluids* **27** 2308–2312.
- HOLLWEG, J. V. 1985 Viscosity in a magnetized plasma - physical interpretation. *J. Geophys. Res.* **90** 7620–7622.
- HOLLWEG, J. V. 1986 Viscosity and the Chew-Goldberger-Low equations in the solar corona. *Astrophys. J.* **306** 730–739.
- HOLZAPFEL, G. A. 2000 Nonlinear solid mechanics: a continuum approach for engineering. Wiley.
- HOOD, A. W., VAN DER LINDEN, R. & GOOSSENS, M. 1989 A formulation of non-ideal localized (or ballooning) modes in the solar corona. *Solar Phys.* **120** 261–283.
- HOOD, A. W., CARGILL, P. J., BROWNING, P. K. & TAM, K. V. 2016 An MHD avalanche in a multi-threaded coronal loop. *Astrophys. J.* **817** 5.
- KOTELNIKOV, I. A. 2012 Braginskii and Balescu kinetic coefficients for electrons in a Lorentzian plasma. *Plasma Phys. Rep.*, **38** 608–619.

- KUNZ, M. W., BOGDANOVIĆ, T., REYNOLDS, C. S. & STONE, J. 2012 Buoyancy instabilities in a weakly collisional intracluster medium. *Astrophys. J.* **754**, 122
- MAC TAGGART, D. & HAYNES, A. L. 2014 On magnetic reconnection and flux rope topology in solar flux emergence. *MNRAS* **438** 1500–1506.
- MAC TAGGART, D., GUGLIELMINO, S. L., HAYNES, A. L., SIMITEV, R. & ZUCCARELLO, F. 2015 The magnetic structure of surges in small-scale emerging active regions. *Astron. & Astrophys.* **576** A4.
- MINOSHIMA, T., MIYOSHI, T. & IMADA, S. 2016 Boosting magnetic reconnection by viscosity and thermal conduction. *Phys. Plasmas* **23** 072122.
- NAPOLI, G. & VERGORI, L. 2012 Surface free energies for nematic shells. *Phys. Rev. E* **85** 061701.
- OFMAN, L., DAVILA, J.M. & STEINOLFSON, R. S. 1994 Coronal heating by the resonant absorption of Alfvén waves: the effect of viscous stress tensor. *Astrophys. J.* **421** 360–371.
- PONTIN, D. I., BHATTACHARJEE, A. & GALSGAARD, K. 2007 Current sheet formation and nonideal behaviour at three-dimensional magnetic null points. *Phys. Plasmas* **14** 052106.
- PRIEST, E. R. 2014 *Magnetohydrodynamics of the Sun*. Cambridge University Press.
- RUDERMAN, M. S., VERWICHTE, E., ERDÉLYI, R. & GOOSSENS, M. 1996 Dissipative instability of MHD tangential discontinuity in magnetized plasmas with anisotropic viscosity and thermal conductivity. *Phys. Plasmas* **56** 285–306.
- SANTOS-LIMA, R., DE GOUVEIA DAL PINO, E. M., KOWAL, G., FALCETA-GONÇALVES, LAZARIAN, A. & NAKAWACKI, M. S. 2014 Magnetic field amplification and evolution in turbulent collisionless magnetohydrodynamics: an application to the intracluster medium. *Astrophys. J.* **781** 84
- SANTOS-LIMA, R., YAN, H., DE GOUVEIA DAL PINO, E. M. & LAZARIAN, A. 2016 Limits on the ion temperature anisotropy in the turbulent intracluster medium. *MNRAS* **460** 2492–2504
- SCHEKOCHIHIN, A. A. & COWLEY, S. C. 2006 Turbulence, magnetic fields and plasma physics in clusters of galaxies. *Phys. Plasmas* **13**, 056501
- SONNERUP, B. U. Ö. & PRIEST, E. R. 1975 Resistive MHD stagnation-point flows at a current sheet. *J. Plasma Phys.* **14** 283–294.
- SPENCER, A. J. M. 1971 Theory of invariants. In *Continuum Physics Vol. 1* (ed. A. C. Eringen), Academic Press, London, pp. 239–353.
- SPITZER, L. & HÄRM, R. 1953 Transport phenomena in a completely ionized gas. *Phys. Rev.* **89** 977–981.
- TAM, K. V., HOOD, A. W., BROWNING, P. K. & CARGILL, P. J. 2015 Coronal heating in multiple magnetic threads. *Astron. & Astrophys.* **580** A122.
- VAN DER LINDEN, R., GOOSSENS, M. & HOOD, A. W. 1988 The effects of parallel and perpendicular viscosity on resistive ballooning modes in line-tied coronal magnetic fields. *Solar Phys.* **115** 235–249.